Pergamon

Geochimica et Cosmochimica Acta, Vol. 68, No. 17, pp. 3497–3507, 2004

0016-7037/04 $30.00 + .00

doi:10.1016/j.gca.2004.02.019

# The oxidation of carbonate green rust into ferric phases:solid-state reaction or transformation via solution

LUDOVIC LEGRAND,[1,*] LÉO MAZEROLLES,[2] and ANNIE CHAUSSÉ[1]

[1]Laboratoire Analyse et Environnement, UMR 8587, CEA-CNRS-Université d'Evry Val d'Essonne, Rue du père Jarland, F-91025 Evry France
[2]Centre d'Etudes de Chimie Métallurgique, CNRS, F-94407 Vitry sur Seine France

(*Received February* 28, 2003; *accepted in revised form February* 18, 2004)

**Abstract**—The oxidation of carbonate green rust, GR($CO_3^{2-}$), in $NaHCO_3$ solutions at T = 25°C has been investigated through electrochemical techniques, FTIR, XRD, TEM and SEM. The used GR($CO_3^{2-}$) samples were made of either suspended solid in solution or a thin electrochemically formed layer on the surface of an iron disc. Depending on experimental conditions, oxidation occurs, with or without major modifications of the GR($CO_3^{2-}$) structure, suggesting the existence of two pathways: solid-state oxidation (SSO) leading to a ferric oxyhydroxycarbonate as the end product, and a dissolution-oxidation-precipitation (DOP) mechanism leading to ferric oxihydroxides such as lepidocrocite, goethite, or ferrihydrite. A formula was proposed for this ferric oxyhydroxycarbonate, $Fe_6^{III}O_{(2+x)}(OH)_{(12-2x)}(H_2O)_x(CO_3)$, assuming that the solid-state oxidation reaction is associated to a deprotonation of the water molecules within the interlayers, or of the hydroxyl groups in the Fe(O,H) octahedra layers. The DOP mechanism involves transformation via solution with the occurrence of soluble ferrous-ferric intermediate species. A discussion about factors influencing the oxidation of carbonate green rust is provided hereafter. The ferric oxyhydroxycarbonate can be reduced back to GR($CO_3^{2-}$) by a reverse solid-state reduction reaction. The potentiality for a solid-state redox cycling of iron to occur may be considered. The stability of the ferric oxyhydroxycarbonate towards thermodynamically stable ferric phases, such as goethite and hematite, was also studied. 

## 1. INTRODUCTION

Green rusts (GRs) are layered Fe(II)-Fe(III) hydroxi-salts that are suspected to occur as minerals in soils alternating redox conditions (Ponnamperuma, 1972; Lindsay, 1979; Taylor, 1980; Trolard et al., 1997). The bluish-green colour of such soils, which turns ochre once exposed to air, would be due to the presence of these mixed-valence compounds. This natural occurrence was postulated on the basis of Mössbauer spectroscopy analysis. Green rusts have also been identified in aerobic/anaerobic corrosion (Butler and Beynon, 1967; Stampfl, 1969; McGill et al., 1976; Génin et al., 1993; Abdelmoula et al., 1996; Bonin et al., 2000; Savoye et al., 2001).

Green rusts belong to the general class of layered double hydroxide (LDH) characterised by a crystalline structure consisting in the stacking of brucite-like layers carrying positive charges and interlayers constituted by anions and water molecules. The structure and the chemical formula of GRs depend upon the specific anions $A^{n-}$ that they incorporate ($A^{n-}$ = $Cl^-$, $SO_4^{2-}$, $CO_3^{2-}$...) (Bernal et al., 1959; Génin et al., 1998). Carbonate green rust, GR($CO_3^{2-}$), has a trigonal structure looking like that of pyroaurite with a stacking sequence *AcBiBaCjCbAkA*..., where *A*, *B*, and *C* represent $OH^-$ planes, *a*,*b*, and *c* Fe(II)-Fe(III) cations layers and *i*,*j*, and *k* intercalated layers (Allmann, 1968). The Fe(II)/Fe(III) ratio usually found for carbonate green rust is (1). (Hansen, 1989) and the chemical formula, $[Fe_4^{II}Fe_2^{III}(OH)_{12}]^{2+}$. $[CO_3^{2-}.m\ H_2O]^{2-}$, should be proposed by analogy with pyroaurite. Previous studies have shown that incorporation of $HCO_3^-$ within the lattice of GR($CO_3^{2-}$) is very improbable, on the basis of FTIR analysis and site availability in interlayers (Benali et al., 2001; Legrand et al., 2001a).

Synthetic GRs have been prepared in the laboratory, using various chemical procedures, from solutions containing ferrous species and chloride ions (Feitknecht and Keller, 1950; Detournay et al., 1976; Refait and Génin, 1993; Schwertmann and Fechter, 1994), ferrous species and sulphate ions (Detournay et al., 1975; Olowe and Génin, 1991; Génin et al., 1996), and ferrous species and carbonate ions (Taylor, 1980; Hansen, 1989; Drissi et al., 1995). Carbonate green rust films have also been obtained from the electrochemical oxidation of iron discs (Legrand et al., 2000).

Recent studies have reported the formation of green rusts from the bioreduction of ferric oxihydroxides by dissimilatory-iron-reducing bacteria (DIRB) (Fredrickson et al., 1998; Ona-Nguema et al., 2002). Such bacteria can use the ferric oxihydroxide as an electron acceptor for the oxidation of organic matter. Ona-Nguema et al. (2002) have shown that large hexagonal crystals of carbonate green rust could be obtained, and they stated that this process may occur in soil solutions and aquifers.

The chemistry and mobility of iron is strongly related to the redox conditions. In environments alternating oxidising and reducing conditions, the cycling of iron will induce oxidation of green rust by dissolved oxygen into ferric products. This oxidation process also occurs when GR interacts with oxidising species such as $NO_3^-$ (Hansen and Bender Koch, 1998), $CrO_4^{2-}$ (Loyaux-Lawniczak et al., 2000; Williams and Scherer, 2001), $CCl_4$ (Erbs et al., 1999), $SeO_4^{2-}$ (Refait et al., 2000), both in natural aquifers and iron permeable reactive barriers (PRBs).

Several studies were dedicated to the characterisation of the products resulting from the oxidation of carbonate green rust. However, the reaction pathways have not been fully under-

* Author to whom correspondence should be addressed (ludovic.legrand@chimie.univ-evry.fr).

stood. Drissi et al. (1995) suggested that the oxidation of GR($CO_3^{2-}$) in $HCO_3^-/CO_3^{2-}$ solutions leads first to a so-called "amorphous active FeOOH" phase distinct from $\alpha$ or $\gamma$-FeOOH. In a recent study, Benali et al. (2001) asserted that this intermediate phase is ferrihydrite, and proposed the following sequence for the oxidation: GR($CO_3^{2-}$) oxidizes into ferrihydrite, and then, ferrihydrite transforms into goethite, $\alpha$-FeOOH, via a dissolution-precipitation mechanism. Taylor (1980), Hansen (1989) and Abdelmoula et al. (1996) studied the oxidation by air of dry samples of carbonate green rust. The formation of feroxyhite, $\delta$-FeOOH, or ferrihydrite was claimed, based on the presence of a line at 0.254 nm in the diffraction pattern. And last, a study by Markov et al. (1990) in which an iron(III) hydroxide carbonate was obtained from the decomposition of siderite in wet air, can also be mentioned.

The aim of the present work is to provide a better description of the oxidation process of carbonate green rust and the resulting ferric products. The transformation of carbonate green rust under various oxidising conditions was studied through electrochemical measurements, X-ray diffraction, FTIR spectroscopy, TEM, and SEM.

## 2. EXPERIMENTAL METHODS

### 2.1. Synthesis and Oxidation of GR($CO_3^{2-}$) Suspension

50 mL of 0.4 or 0.04 mol/L $NaHCO_3$ solution (prepared with $NaHCO_3$ as received from Fluka, purity >99.5%, and 18 MΩ cm nano-pure water) were introduced in a glass cell (~50 mm diam.) with five holes on the top. Three of the holes were used for the electrodes: platinum electrode, saturated calomel electrode (0.25 $V_{SHE}$), and combined pH electrode (WTW sentix 41). Another hole was used for the argon inlet and outlet. The fifth hole 15 mm diameter), located in the middle position, was closed by a rubber cap during the deaeration of the solution; for the aeration of the solution, the argon flow was stopped and the rubber cap was removed to allow the air oxygen to get in contact with the solution at the air/liquid interface. The solution was magnetically stirred (300 rpm) and thermostated at 25°C during the chemical procedure. The solution/air interface was ~20 $cm^2$ in area. Before Fe(II) addition, the $NaHCO_3$ solution was deaerated with argon, (argon U, Air liquide, ~20 mL $min^{-1}$) whose residual oxygen content was eliminated by bubbling in a $Fe(OH)_2$ suspension present in the liner before injection into the cell. Then 0.5 mL (giving an initial Fe(II) concentration of $10^{2-}$ M) of a 1 mol/L $FeCl_2$ solution was injected into the solution using a syringe through the rubber cap. To get an appropriate initial pH value, 10 mol/L (or 1 mol/L) NaOH solution was dropped into the preparation. $FeCl_2$ solution was prepared by dissolving the appropriate amount of $FeCl_2$, $4H_2O$ from Aldrich (purity 99%) in deaerated 18 MΩ cm nano-pure water. The oxidation reaction was monitored by recording both redox potential ($E_h$) and pH of the solution. A millivoltmeter (Taccusel minisis 8000) and a pHmeter (WTW multiline P4) were used. In some experiments, hydrogen peroxide was also used as an oxidising species. A 1 mol/L solution was prepared with 30% $H_2O_2$ commercial solution (as received from Sigma) and 18 MΩ cm nano-pure water.

### 2.2. Electrochemical Studies of GR($CO_3^{2-}$) Thin Layer On Iron

Electrochemical measurements were performed in a cylindrical cell containing ~15 mL of solution. A 15 mm diameter iron disk (99.5% purity, provided by Goodfellow) was used as a working electrode; a large surface-area platinum grit was used as a counter electrode; an AgCl-coated silver wire immersed in a compartment with a fine porosity glass frit and filled with 0.1 mol/L NaCl was used as a reference electrode (0.28 $V_{SHE}$). The iron disk was polished on abrasive foils from grade 500 to grade 4000 and rinsed with 18 MΩ cm nano-pure water before use. The iron disk was then placed at the bottom of the cell. The surface in contact with the electrolyte was measured as 0.785 $cm^2$. Electrolyte solutions were deaerated with argon for 15 min before electrolysis, and the argon bubbling was maintained during the whole electrochemical measurements.

Electrochemical preparation and investigations were performed using a potentiostat PAR 273 A controlled by an IBM computer and the PAR Model 270 software package. The electrochemical synthesis of GR($CO_3^{2-}$) layer was done by applying an anodic potential (−0.45 $V_{SHE}$) to the iron disk in 0.4 mol/L $NaHCO_3$ solution at pH = 9.6. The electrolysis was stopped as the current density became lower than 10 $\mu A\ cm^{-2}$, indicating that the electrode surface was fully covered by the GR($CO_3^{2-}$) particles. The coulombic charge required for this purpose was ~150 mC $cm^{-2}$. More details about the electrochemical synthesis and FTIR analysis of GR($CO_3^{2-}$) layers can be found in Legrand et al. (2001a and 2001b).

### 2.3. Characterisation of Solid Products

XRD measurements were carried out by using a Philips PW1830 diffractometer with a Co $K_\alpha$ radiation (1.7902 Å). The samples were scanned from 5° to 90° 2$\theta$. FTIR data were recorded on a Bruker IFS 28 Fourier Transform Infrared spectrometer. Powder samples were pressed to pellets with KBr and analysed by direct transmission mode. Electrochemically formed layers on the surface of the iron disk were directly analysed using a reflection transmission tool (Grazeby-Specac). 20 scans were done for the spectrum acquisition and the acquisition time was ~30 s. TEM measurements were performed with a JEOL 2000FX operating at 200kV. A double-tilt ±30° specimen holder was used, and observations were directly achieved on powders deposited on copper grids. SEM measurements were performed with a Philips XL30 microscope.

Solid products, resulting from chemical synthesis, were separated from the solutions by collecting on 0.22 $\mu$m Millipore filters under argon atmosphere. They were rinsed with deaerated nano-pure water. The filters were then quickly removed from the filtration tool and introduced into a closed glass tube equipped with argon inlet and outlet for drying. The solid products were maintained under argon flow for ~1 h before analysis. In the case of the intermediate product (carbonate green rust), the preparation of the KBr pellets for FTIR measurements was done under argon atmosphere to avoid oxidation by air. For XRD measurements, the intermediate product was protected from air oxidation by admixing glycerol, once filtered (Hansen, 1989). Oxidation products electrochemically formed at the surface of an iron disk were washed with deaerated 18 MΩ cm nano-pure water, dried under argon flow, and quickly introduced into the chamber for FTIR or SEM analysis. The contact with air was less than 1 min.

The following procedure was used to determine the Fe(II) content in solid suspensions at a given time. After removal of air by argon purge to stop the oxidation, the solution was acidified with concentrated $H_2SO_4$ down to a pH of ~0.5 to induce the dissolution of the solid phases. Titration of $Fe^{2+}$ ions was done with a 0.01 mol/L $KMnO_4$ solution.

The total iron content was assessed by two methods. The first one consists in a complexometric titration of Fe(III) by ethylene diamine tetraacetic acid (EDTA from Prolabo, normapur). 50 mg of dried solids (50 mg) are dissolved in hot 1 mol/L HCl (~5–7 mL). After complete dissolution, 18 MΩ cm nano-pure water is added until a volume of 50 mL si reached. The solution is then thermostated at 45°C, and 3 drops of sulfosalicilic acid indicator are added. The equivalent volume of EDTA (0.05 mol/L) is measured when the colour changes from dark purple to light yellow. In the case of GR($CO_3^{2-}$), 2 mmol of $H_2O_2$ are added to the solution before titration, to oxidise $Fe^{2+}$ ions into $Fe^{3+}$ ions. The second method consists in hematisation (i.e., transformation of the product into hematite, $\alpha$-$Fe_2O_3$). The dried product is first weighted ($m_0$) and then heated to 300°C for 40 h. After this treatment, the product is fully transformed into hematite, whose mass can be determined ($m_H$). The mass of iron, $m_{Fe}$, is equal to $0.699m_H$. Finally, the total Fe content in the solid product is determined by the $m_{Fe}$ to $m_0$ ratio. It has to be noted that the complete transformation into hematite is controlled by FTIR.

The $CO_2$ content in the solid samples was determined by acid-base titration. A weighted amount of dried solid sample (in the 52–57 mg range) was introduced into an inner glass tube (~10 mL) located in an outer glass tube (~50 mL) filled in with 5 mL of 0.1 mol/L NaOH solution; the latter solution was prepared from 30% NaOH solution (RP

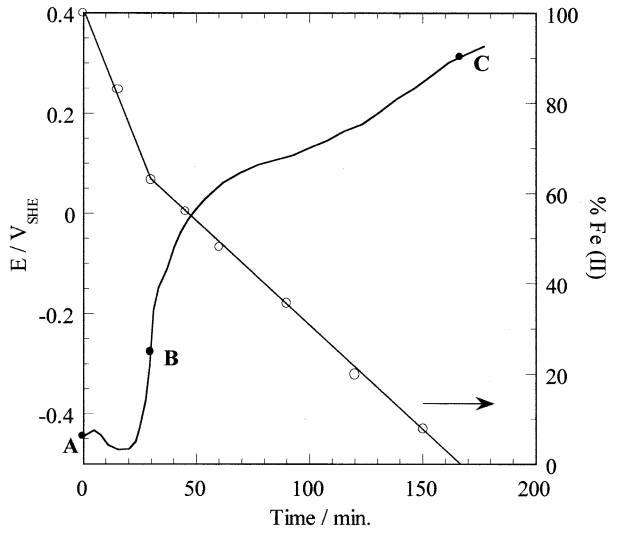


Fig. 1. E vs. time and %Fe(II) vs. time recorded during oxidation by air of $10^{-2}$ M Fe(II) suspension in 0.4 mol/L $NaHCO_3$ solution; pH = 9.6; T = 25°C; stirring 300 rpm.

Prolabo) containing less than 1% of $Na_2CO_3$ impurity. Both tubes were equipped with a magnetic bar. The inner tube was maintained open while the outer one was closed by a gas-proof rubber stopper. Then, 7 mL of 1 mol/L HCl solution were injected into the inner tube through the stopper by using a syringe. The tubes were settled on a magnetic stirrer (300 rpm) for 5 h. The suspended solid completely dissolved within 3 h. $CO_2$ resulted from the dissolution and was absorbed in NaOH solution. $CO_2$ was then determined by acid/base titration of the carbonated NaOH solution. Note that the blank titration was carried out and the $CO_2$ content of the 0.1 mol/L NaOH solution was subtracted from the experimental values.

## 3. RESULTS

### 3.1. Synthesis and Oxidation of GR($CO_3^{2-}$) Suspension In 0.4 mol/L $NaHCO_3$ Solution

#### *3.1.1. E-t and pH-t transients*

Figure 1 reports the potential values recorded with a platinum electrode as a function of time during the aerial oxidation of a Fe(II) suspension in 0.4 mol/L $NaHCO_3$ solution with an initial pH = 9.6, and the corresponding evolution of Fe(II) content, expressed as a percentage. Oxidation occurs in two steps separated by a potential jump. The potential jump indicates the end of the first step, corresponding to the complete consumption of the initial ferrous suspension. Analysis done at point B indicates that the Fe(II) content is ~66%. The colour of the suspension changes from white to dark green (from A to B), then to greenish-brown, and finally to light brown colours (from B to C). From A to C, the pH does not significantly change. No potential jump is observed at the end of the second step, but Fe(II) titration indicates that the formation of the ferric product gets completed at point C (0% of Fe(II)). The average oxidation rates for the A-to-B and B-to-C steps are 6.0 and 2.3 $\mu$moles $Fe^{II}$ $min^{-1}$, respectively. Experiments performed at different initial pH values in the 8.8 to 10.5 range gave E-t transients similar to that reported in Figure 1.

#### *3.1.2. Characterisation of solid products*

Figure 2 gives the XRD patterns of the products obtained at points A, B, and C. The initial ferrous suspension (a) is amorphous as shown by the lack of diffraction lines. Figure 2b exhibits typical lines of a pyroaurite-like green rust structure (Allmann, 1968). Following lattice parameter values were calculated assuming a rhombohedral R$\bar{3}$m structure,

$$a = 0.3172 \pm 0.0005 \text{ nm}$$

and

$$c = 2.274 \pm 0.0\,3 \text{ nm}.$$

They are consistent with those reported in the literature for carbonate green rust GR($CO_3^{2-}$) (McGill et al., 1976; Taylor, 1980; Hansen, 1989; Drissi et al., 1995; Legrand et al., 2001a). As GR($CO_3^{2-}$) belongs to the R$\bar{3}$m group, c parameter indicates a 0.758 nm interplanar distance between $Fe^{2+}$-$Fe^{3+}$ layers. XRD pattern of the ferric product, sampled at point C (Fig. 2c), displays a main line, corresponding to an interplanar distance of 0.734 nm. Some minor lines at 0.367 nm (0.734/2), 0.253 nm, and 0.226 nm are also observed. Such a diagram has already been reported in the literature for GR($CO_3^{2-}$) powders oxidised by air in dry conditions (Taylor, 1980; Hansen, 1989; Abdelmoula et al., 1996). The 0.734 nm interplanar distance value may indicate that some relics of the lamellar structure of the parent GR($CO_3^{2-}$) remain in the Fe(III) product structure obtained at point C. Since the ionic radii of $Fe^{2+}$ and $Fe^{3+}$ are 0.078 and 0.0645 nm, respectively, the difference between 0.734 nm and 0.758 nm could be related to a contraction in the

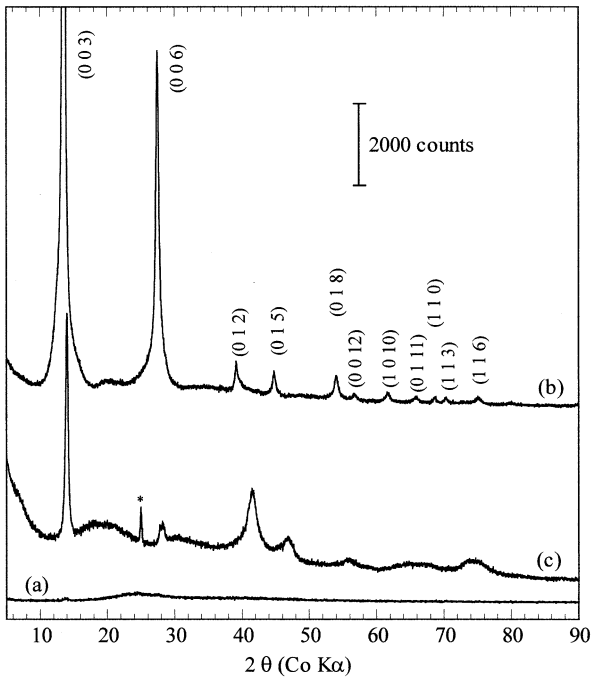


Fig. 2. XRD patterns of (a) the starting ferrous suspension sampled at point A; (b) the product sampled at point B, GR($CO_3^{2-}$); and (c) the ferric product sampled at point C, exGR-Fe(III). (* goethite as a trace). Step time (a and b) 3 s; (c) 5 s; step size 2$\theta$ (a and b) 0.025°; (c) 0.03°.

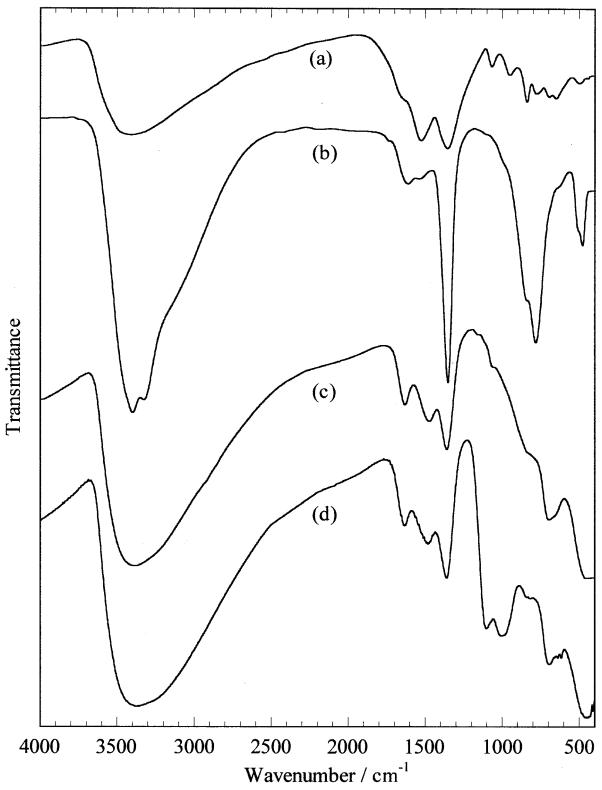


Fig. 3. FTIR spectra of (a) the starting ferrous suspension sampled at point A; (b) the product sampled at point B, GR($CO_3^{2-}$); (c) the ferric product sampled at point C, exGR-Fe(III); and (d) the ferric product sampled at point C, following the same procedure as given in Figure 1, except that $10^{-2}$ M $Na_2HPO_4$ was added at point B.

solid lattice induced by the $Fe^{2+}$-to-$Fe^{3+}$ transformation (Abdelmoula et al., 1996). Moreover, the small variation of the interplanar distance might be consistent with the presence of $CO_3^{2-}$ anions in the interlayers of the Fe(III) product. The ferric product sampled at point C will thereafter be referred as exGR-Fe(III).

The FTIR spectrum of the initial ferrous suspension (Fig. 3a) exhibits bands at 1530, 1355, 1075, 955, 840, 780, and 760 $cm^{-1}$, that have already been reported for ferrous hydroxicarbonate, $Fe_2(OH)_2CO_3$, (Erdös and Altorfer, 1976). The broadness of the IR bands is consistent with the amorphous nature of the solid product, as pointed out by XRD. The FTIR spectrum of the product formed at point B (Fig. 3b) exhibits only the GR($CO_3^{2-}$) bands: i.e., $H_2O$ and -OH stretching modes at 3500, 3410, 3310 $cm^{-1}$, and 3170 $cm^{-1}$; $H_2O$ bending vibration ($\delta$) at 1630 $cm^{-1}$; $CO_3^{2-}$ stretching modes at 1350 ($\nu_3$); and lattice Fe-OH modes at 845, 770, 510, and 480 $cm^{-1}$ (Taylor, 1980; Legrand et al., 2001b, Peulon et al., 2003). The lack of the 1070 and 955 $cm^{-1}$ bands in spectrum (b) is consistent with the complete removal of the initial ferrous suspension. The FTIR spectrum of the exGR-Fe(III) product is given in Figure 3c. The 470 and 655 $cm^{-1}$ bands are assigned to stretching Fe-O modes in octahedral Fe-O(OH) coordination (Markov et al., 1990). The broad band between 2300 and 3600 $cm^{-1}$, attributed to OH stretching vibrations in water molecules and hydroxyl groups, is the sum of three contributions located at 3465, 3290, and 3020 $cm^{-1}$. The absorption at 1635 $cm^{-1}$ is assigned to the bending vibration of water. The presence of $CO_3^{2-}$ ions is revealed by the two strong absorption bands at 1360 ($\nu_3$) and 690 $cm^{-1}$ ($\nu_4$) and two much weaker ones at 1070 ($\nu_1$) and 850 $cm^{-1}$($\nu_2$). The symmetry of $CO_3^{2-}$ deviates from $D_{3h}$ as seen from the splitting of the $\nu_3$ mode (1360 and 1480 $cm^{-1}$) and from the observation of the normally IR-forbidden $\nu_1$ absorption. To prove that $CO_3^{2-}$ anions are inside the lattice rather than adsorbed species, an exGR-Fe(III) sample was synthesized according to the same procedure as given in Figure 1, except that $10^{-2}$ M $Na_2HPO_4$ was added at point B. The final product is also exGR-Fe(III), as revealed by XRD (pattern not shown) and FTIR analysis (Fig. 3d). The adsorption of phosphate species is indicated by the antisymmetric $\nu_3$ $PO_4$ stretching (1000 and 1105 $cm^{-1}$) and $\nu_4$ $PO_4$ deformation (620 and 640 $cm^{-1}$) modes, which split due to the monodentate or bidentate coordination to the oxo or hydroxo-groups. The carbonate bands are not affected by the presence of adsorbed phosphate species.

The transmission electron microscopy image of exGR-Fe(III) is given in Figure 4. It shows a hexagonal platelets morphology identical to that commonly reported in the literature for green rust (McGill et al., 1976; Legrand et al., 2001a; Géhin et al., 2002; Peulon et al., 2003), suggesting a solid-state oxidation of carbonate green rust into exGR-Fe(III). The electron diffraction studies exploring the reciprocal lattice did not allow us to identify the structure of this phase due to the very anisotropic morphology of these platelets. This anisotropy limits the variety of cristallographic planes which can be studied, and it is not possible to measure the c parameter that is perpendicular to the observation plane.

Table 1 reports the results of chemical analysis of GR($CO_3^{2-}$) and exGR-Fe(III) samples and the data computed for some ferric oxihydroxides that should be expected according to the literature (see Introduction). The total Fe and $CO_2$ contents of GR($CO_3^{2-}$) and exGR-Fe(III) compare quite well. The theoretical values calculated for ferrihydrite and feroxyhyte do not match at all with the experimental data obtained for exGR-Fe(III).

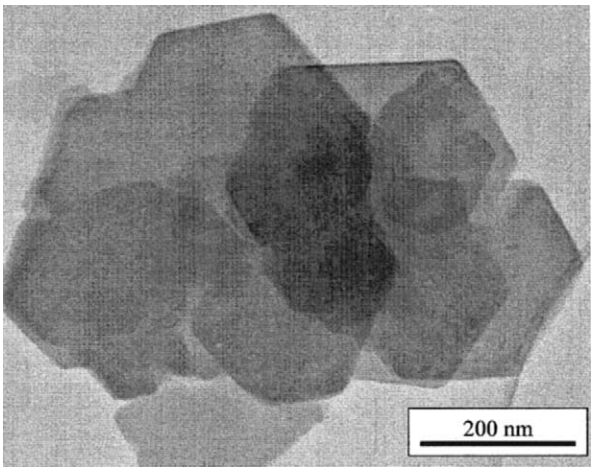


Fig. 4. TEM image of the ferric product sampled at point C, exGR-Fe(III).

Table 1. Chemical analysis data of products sampled at point B, GR($CO_3^{2-}$), and at point C, exGR-Fe(III). Comparisons of experimental data of exGR-Fe(III) with theoretical data of ferrihydrite and feroxyhyte.

| | | Total Iron Content (% wt) | | |
|---|---|---|---|---|
| | Fe(II)[a] (%) | EDTA | Hematisation | $CO_2$ Content (% wt) |
| GR($CO_3^{2-}$) samples taken at point B | 66 ± 2 (4) | 51.2 ± 0.2 (3) | 52.9 ± 0.3 (3) | 5.8 ± 0.2 (3) |
| Carbonate green rust[b] | 67 | 52.8 | | 6.9 |
| ExGR-Fe(III) samples taken at point C | 0 (1) | 50.1 ± 0.4 (5) | 53.4 ± 0.6 (3) | 5.0 ± 0.2 (4) |
| Ferrihydrite[c] | 0 | 58.2 | | 0 |
| Feroxyhyte[d] | 0 | 62.9 | | 0 |

In brackets, we give the number of samples that were analyzed. Each value was obtained from one solid sample synthesized according to the procedure given in Figure 1 (point B or C). An average value and the corresponding standard deviation were then calculated.

[a] $KMnO_4$ titration; Fe(II)% = nFe(II)/n(total iron).

[b] Theoretical values calculated by assuming the formula $[Fe_4^{II}Fe_2^{III}(OH)_{12}]$ $[CO_3, 2H_2O]$ given by Drissi et al. (1995).

[c] Theoretical values calculated by assuming the formula $Fe_5HO_8.4H_2O$ given by Towe and Bradley (1967).

[d] Theoretical values calculated by assuming the formula δ-FeOOH given by Chukhrov et al. (1977).

### 3.2. Synthesis and Oxidation of GR($CO_3^{2-}$) Suspension In 0.04 mol/L $NaHCO_3$ Solution

#### *3.2.1. E-t and pH-t transients*

Experiments were done in solutions with lower $NaHCO_3$ concentration to address compositions more closely simulating groundwater or aquifers. Figure 5a reports the E-t and pH-t curves recorded during the oxidation of an Fe(II) suspension in 0.04 mol/L $NaHCO_3$ solution at initial pH = 8.6. The step A-B corresponds to the oxidation of the initial Fe(II) suspension into GR($CO_3^{2-}$), as revealed by the dark green colour of the suspension at point B, and FTIR analysis. The average oxidation rate, 5.6 $\mu$moles $Fe^{II}$ $min^{-1}$, is very close to that determined in Figure 1. A pH decrease from 8.6 to 7.5 is observed during this step. The oxidation of GR($CO_3^{2-}$) into ferric product takes place from B to C. The shape of the E-t transient from B to C strongly differs from what has been recorded during the oxidation experiment reported in Figure 1. Moreover, the average oxidation rate, 5.8 $\mu$moles $Fe^{II}$ $min^{-1}$, is 2 to 3 times larger than that of Figure 1. The FTIR analysis of the solid product obtained at point C (Fig. 5b) shows the characteristic bands of lepidocrocite, γ-FeOOH, at 745, 1020, 1155, 2800 and 3150 $cm^{-1}$ (Schwertmann and Cornell, 1991; Weckler and Lütz, 1998), suggesting that another oxidation mechanism occurs. A small quantity of goethite is also detected (see shoulders at ~900 and 800 $cm^{-1}$). Moreover, the formation of ferrihydrite cannot reasonably be excluded.

#### *3.2.2. Influence of pH on GR($CO_3^{2-}$) oxidation*

Some experiments similar to the one described in Figure 5a were carried out at different starting pH values, and consequently at different pH values during the step from B to C. The ferric products formed at point C were identified by means of FTIR and XRD measurements. Figure 6 indicates the ferric products that were obtained as a function of the pH range recorded during the B-to-C step. For pHs lower than 8, the formation of lepidocrocite is favoured. For pHs greater than 8.9, only exGR-Fe(III) is formed. For pHs between 8 and 8.9, a mixture of both lepidocrocite and exGR-Fe(III) is obtained.

#### *3.2.3. Influence of the rate of GR($CO_3^{2-}$) oxidation*

Figure 7a reports the same experiment as Figure 5a, except that the stirring rate was increased from 300 to 700 rpm at point B. The increase of the stirring rate induces an increase of the oxygen supply, and then a decrease of the time duration of the

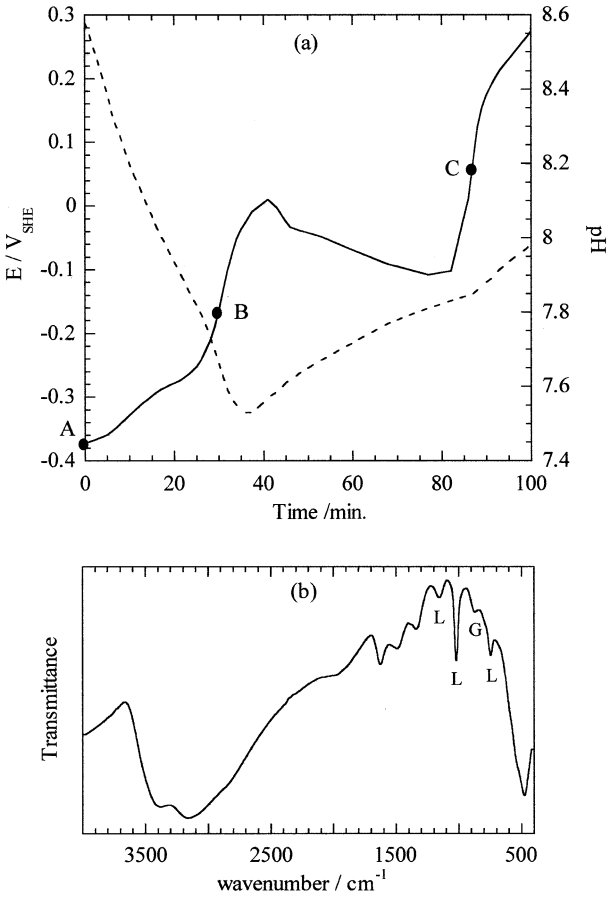


Fig. 5. (a) E-t and pH-t curves recorded during the oxidation by air of $10^{-2}$ M Fe(II) suspension in 0.04 mol/L $NaHCO_3$ solution, starting pH = 8.6, T = 25°C, stirring 300 rpm; (b) FTIR spectrum of the ferric product obtained at point C, L = lepidocrocite; G = goethite.

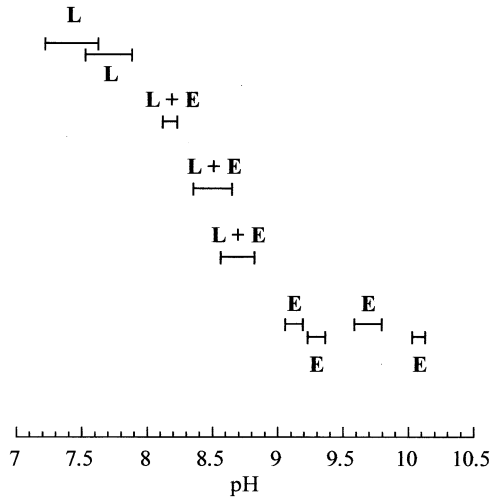


Fig. 6. Influence of pH on the nature of predominant ferric products obtained at point C in 0.04 mol/L $NaHCO_3$ solution; T = 25°C; stirring 300 rpm. E = exGR-Fe(III); L = lepidocrocite.

B-to-C step (26 min. in Fig. 7a against 57 min. in Fig. 5a). ExGR-Fe(III) is predominantly formed at the completion of oxidation (Fig. 7c); only a very small amount of lepidocrocite can be detected.

Another set of experiments in which $H_2O_2$ was used as a soluble, strongly oxidizing species, was done in 0.04 mol/L $NaHCO_3$ solutions with starting pHs in the 7 to 10 range. At point B, the cell was closed, placed under argon bubbling, and 0.25 mL of 1 mol/L $H_2O_2$ (i.e., 5 $10^{-3}$ M) was added to $GR(CO_3^{2-})$ suspension. Figure 7b gives typical E-t and pH-t transients. A sharp increase of potential in less than 1 min, along with a colour change from dark green to light brown is observed, indicating the oxidation completion. The ferric product is exGR-Fe(III), whatever the starting pH (FTIR spectrum not shown). Finally, in an experiment where a dried $GR(CO_3^{2-})$ powder was left in contact with air, the final ferric product was also exGR-Fe(III).

### *3.2.4. Influence of blocking adsorbed species on the oxidation of GR($CO_3^{2-}$)*

Figure 8 reports the same experiment as in Figure 5a, except that $10^{-2}$ M $Na_2HPO_4$ was added at point B. The addition of $HPO_4^-$ ions affects the shape of the B-to-C step, as compared to Figure 5a—a sharp increase of E followed by a potential plateau near 0.2 V is obtained. This shape is similar to that of Figure 1. Analysis of the ferric product formed at point C was carried out by FTIR. The spectrum (not shown) indicates that it is exGR-Fe(III) with phosphate species adsorbed at the surface (a spectrum resembling the one of Fig. 3d is obtained). Some similar experiments performed at different pH values in the 7 to10 range also gave the same final ferric product. On the other hand, the formation of lepidocrocite became inhibited. ExGR-Fe(III) with silicate species adsorbed at the surface was obtained in solutions where $Na_2SiO_3$ was added instead of $Na_2HPO_4$. Note that the substitution of carbonate ions for phosphate or silicate ions inside $GR(CO_3^{2-})$ interlayers is not considered (Benali et al., 2001).

### 3.3. Acid Titration of GR($CO_3^{2-}$) Suspension

Figure 9 reports the results of acid titration of 0.04 mol/L $NaHCO_3$ solutions (50 mL) with (curve (a)) or without (curve (b)) 1.67 mM $GR(CO_3^{2-})$ suspension. Curve (a) was obtained as follows: 1 mol/L NaOH was added to a 0.04 mol/L $NaHCO_3$ solution until pH reached 11.3. Then, $10^{-2}$ M $FeCl_2$ was added and the pH decreased down to 10.4. The conversion of the starting ferrous suspension (10 mM) into $GR(CO_3^{2-})$ suspension (1.67 mM = 10/6) was done by air oxidation (step A to B). At point B, the pH was 10.2. The cell was closed and placed under Ar bubbling and then, the acid titration of the solution + $GR(CO_3^{2-})$ suspension was performed. The blank curve (b) was obtained from the acid titration of a 0.04 mol/L $NaHCO_3$ + NaOH solution with initial pH of 10.2. At first, both curves exhibit the neutralization of $CO_3^{2-}$ species in the 10 - 9 pH range. A pH pseudoplateau at ~8.4, that should be attributed to

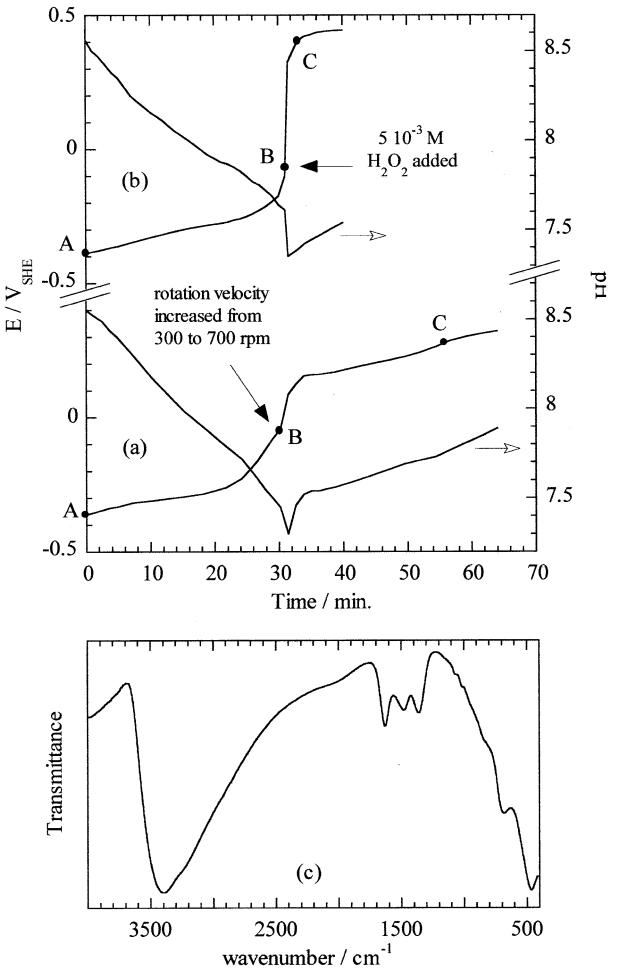


Fig. 7. (a) E-t and pH-t curves recorded during the oxidation by air of $10^{-2}$ M Fe(II) suspension in 0.04 mol/L $NaHCO_3$ solution, starting pH = 8.6, T = 25°C. From A to B, stirring 300 rpm, beyond B, stirring 700 rpm; (b) E-t and pH-t curves recorded during the oxidation of $10^{-2}$ M Fe(II) suspension in 0.04 mol/L $NaHCO_3$ solution, starting pH = 8.6, T = 25°C, stirring 300 rpm. From A to B, oxidation by air. At point B, the cell was placed under argon bubbling and 5 $10^{-3}$ M $H_2O_2$ were added (0.25 mL of 1 mol/L $H_2O_2$); (c) FTIR spectrum of the ferric product, exGR-Fe(III), obtained at point C in curve (a).

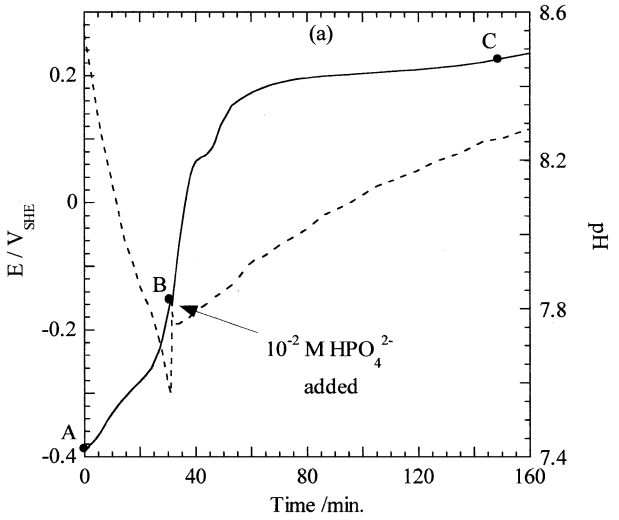


Fig. 8. E -t and pH -t curves recorded during the oxidation by air of $10^{-2}$ M Fe(II) suspension in 0.04 mol/L $NaHCO_3$ solution, starting pH = 8.6, T = 25°C, stirring 300 rpm. $10^{-2}$ M $Na_2HPO_4$ were added at point B.

the acid-induced dissolution of GR($CO_3^{2-}$) suspension, is observed in curve (a). The volume of acid can be estimated to 4 mL, corresponding to an addition of 4.8 mol $H^+$ with respect to one mole GR($CO_3^{2-}$). Note that the pH values recorded during the pseudoplateau are not strictly equilibrium values, mainly due to the too large rate of HCl addition, 0.05 mL $min^{-1}$.

### 3.4. Solid-State Redox Cycling of GR($CO_3^{2-}$)/exGR-Fe(III) System

GR($CO_3^{2-}$) thin layers were electrochemically synthesized at the surface of an iron disk as described in part 2.2. Figure 10a shows the morphology of a layer after its oxidation by dissolved oxygen in an aerated 0.01 mol/L $NaHCO_3$ + 0.001 mol/L $Na_2HPO_4$ solution at pH = 8.5. ExGR-Fe(III) is formed (see FTIR spectrum (c1) in Fig. 10c); no change of the layer morphology is observed, as compared to the starting GR($CO_3^{2-}$) particles. The hexagonal particles obtained from electrochemical synthesis have significantly larger sizes than those obtained from a suspension (compare Figs. 4 and 10a). Figure 10b reports the E-t transient obtained during the galvanostatic reduction of an exGR-Fe(III) layer in simulated groundwater. A plateau is observed, indicating the occurrence of the exGR-Fe(III) reduction process. The potential values recorded on the plateau are close to -0.4 V. The completion of exGR-Fe(III) reduction is revealed by the sharp decrease of the potential (time ~ 4500 s), down to a range corresponding to the electrolyte reduction. The FTIR analysis of the layer, performed after the galvanostatic reduction (Fig. 10c, spectrum

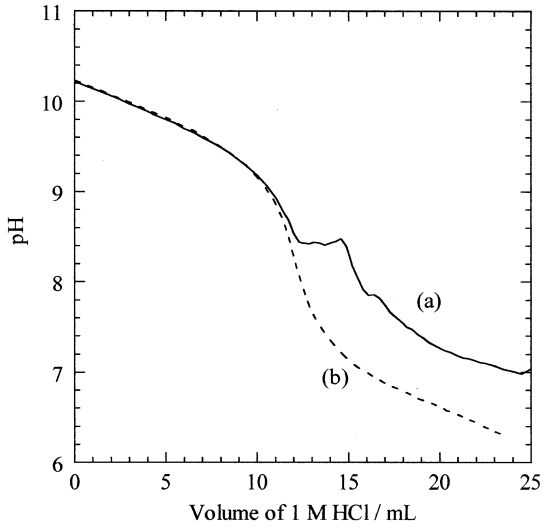


Fig. 9. 0.1 mol/L HCl acid-titration curve of 0.04 mol/L $NaHCO_3$ solution containing (a) 1.67 mM of GR($CO_3^{2-}$) suspension; (b) no GR($CO_3^{2-}$).

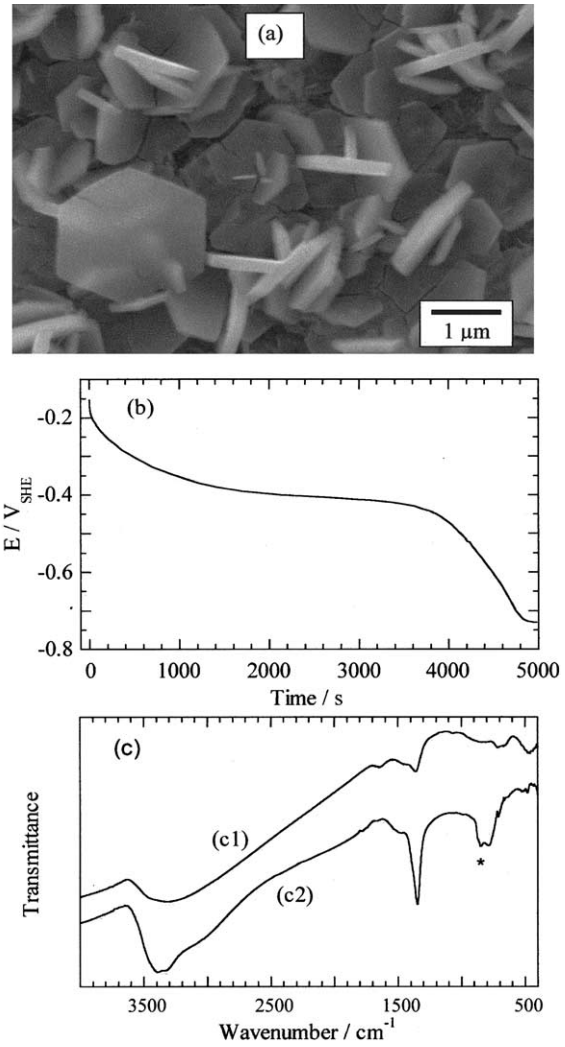


Fig. 10. (a) SEM image of an exGR-Fe(III) thin layer on iron disk; (b) E-t transient recorded during the galvanostatic reduction (- 10 $\mu$A) of an exGR-Fe(III) thin layer in deaerated $CaCO_3$ 2 $10^{-3}$ M + 2 $10^{-2}$ M NaCl solution at 25°C; (c) FTIR analysis of the disk surface before (c1) and after (c2) galvanostatic reduction. (c1) exGR-Fe(III); (c2) GR($CO_3^{2-}$); (*) traces of calcite.

Table 2. Stability or conversion of exGR-Fe(III) under various wet aging conditions Polytetrafluoroethylene (PTFE).

| Initial | Solution | Container | pH | T°C | Storage Time | Final |
|---|---|---|---|---|---|---|
| Dried powder | $10^{-2}$ M $NaHCO_3$ | Teflon | 8.5 | 25 | 24 days | ExGR-Fe(III) + traces of goethite |
| Dried powder | $10^{-2}$ M $NaHCO_3$ | Teflon | 8.5 | 60 | 8 days | Goethite |
| Dried powder | $H_2O$ | Teflon | 8.5 | 60 | 8 days | Goethite |
| Suspension left in solution after synthesis | 0.4 M $NaHCO_3$ | Teflon | 9.6 | 60 | 8 days | Hematite + goethite |
| Suspension left in solution after synthesis | 0.4 M $NaHCO_3$ | Glass | 9.6 | 50 | 40 days | ExGR-Fe(III) + detection of adsorbed silicate ions |
| Dried powder | $10^{-2}$ M $NaHCO_3$ +$10^{-3}$ M $Na_2HPO_4$ or $Na_2SiO_3$ | Teflon | 8.5 | 60 | 8 days | ExGR-Fe(III) + adsorbed phosphate or silicate ions |

(c2)) shows the complete transformation of exGR-Fe(III) into GR($CO_3^{2-}$), involving a solid-state reduction.

### 3.5. Stability of exGr-Fe(III) In Solution

ExGR-Fe(III) samples were stored in solutions for several days, and solids were then analysed by means of FTIR or XRD. Results are computed in Table 2. At 25°C, the conversion of exGR-Fe(III) is very slow since only traces of goethite, $\alpha$-FeOOH, are observed after 24 d aging. At 60°C, when the suspensions are stored in a PTFE vessel (no silicate ions), the complete conversion into goethite or into a hematite ($\alpha$-$Fe_2O_3$) and goethite mixture occurs. When phosphate (or metasilicate) ions are introduced at the beginning of the storage, or when a glass container is used, exGR-Fe(III) does not transform due to the adsorption of phosphate or silicate species (see Fig. 3d) which inhibit the dissolution step needed for the formation of goethite.

## 4. DISCUSSION

### 4.1. Carbonate Green Rust GR($CO_3^{2-}$)

The specific surface area of the Fe(II) suspension might be very large due to its amorphous state; this feature warrants an easy dissolution and a flow of soluble $Fe^{II}$ species large enough to compensate the flow of dissolved oxygen. This fact is supported by the rather stable potential values that are recorded along the A-to-B oxidation step. The oxidation of the soluble $Fe^{II}$ species supplied by the amorphous Fe(II) suspension might lead to the production of soluble ferrous-ferric intermediate species, whose occurrence has previously been claimed by Misawa et al. (1973 and 1974). According to these authors, the following schematic formula may be proposed $[(Fe^{II})_2(Fe^{III})_1]$. The precipitation of GR($CO_3^{2-}$) occurs as the concentration of $[(Fe^{II})_2(Fe^{III})_1]$ species exceeds the solubility limit. From Table 1, the following formula for GR($CO_3^{2-}$) can be proposed (see Appendix for details),

$$Fe^{II}_{3.96}Fe^{III}_{2.04}(OH)_{12.34}(CO_3)_{0.85}(H_2O)_{2.62}\,. \qquad (2)$$

The formula is consistent with those reported by Hansen (1989), Stampfl (1969) and Drissi et al. (1995), $[Fe^{II}{}_4Fe^{III}{}_2(OH)_{12}]$ $[CO_3, mH_2O]$, with $m$ likely equal to (2).

### 4.2. Solid-State Oxidation of GR($CO_3^{2-}$)

#### *4.2.1. ExGR-Fe(III), a ferric oxyhydroxycarbonate*

The exGR-Fe(III) product resulting from the solid-state oxidation (SSO) of GR($CO_3^{2-}$) exhibits a light brown colour and a hexagonal platelets morphology. Table 1 indicates that its composition is very close to that of GR($CO_3^{2-}$). From the results of Table 1 and the charge balance (see Appendix for details), the chemical composition of exGR-Fe(III) can be proposed, $(Fe^{III})_6(O)_{14.41}(H)_{12.30}(CO_3)_{0.74}$. The presence of remaining carbonate ions inside the exGR-Fe(III) crystal lattice is fully demonstrated in this study. Replacing O and H contents by $O^{2-}$, $OH^-$, and $H_2O$, the following formula can be proposed, $Fe^{III}{}_6O_{(2.11+x)}(OH)_{(12.30-2x)}(H_2O)_x(CO_3)_{0.74}$. Hence, ExGR-Fe(III) is a ferric oxyhydroxycarbonate. Finally, the assumption that the solid-state oxidation of GR($CO_3^{2-}$) gives ferrihydrite or feroxyhyte (Taylor, 1980; Hansen, 1989; Abdelmoula et al., 1996) must be revisited.

#### *4.2.2. Deprotonation as a way for keeping electrical neutrality*

The solid-state oxidation (SSO) of GR($CO_3^{2-}$) involves the transformation of $Fe^{2+}$ ions into $Fe^{3+}$ ions inside the crystal lattice. The formula of GR($CO_3^{2-}$) can be written as follows: $[Fe^{II}{}_4Fe^{III}{}_2(OH)_{12}]$ $[CO_3, 2H_2O]$. This last formula and the corresponding molar mass 635.1 g $mol^{-1}$ can be admitted for our GR($CO_3^{2-}$). The solid-state oxidation implies charge compensation to satisfy the electrical neutrality of the whole structure. The compensation by some anionic species during GR($CO_3^{2-}$) oxidation can be ruled out since the number of interlayer sites required for this purpose would be greater than the available sites (Legrand et al., 2003). The loss of protons to accommodate the charge compensation is more consistent with the results of Table 1. The solid-state oxidation (SSO) of GR($CO_3^{2-}$) can be written as:

$$[Fe^{II}_4Fe^{III}_2(OH)_{12}][CO_3, 2H_2O] \rightarrow Fe^{III}_6O_{(2+x)}(OH)_{(12-2x)} \times (H_2O)_x(CO_3) + 4H^+ + 4e^- \qquad (3)$$

The value of x depends on whether or not the deprotonation of interlayer water molecules to give $OH^-$ ions is considered. Eqn. 3 shows that exGR-Fe(III) is obtained from the release of 4 protons and 4 electrons by GR($CO_3^{2-}$). Combining Eqn. 3 with the reduction reaction of $O_2$ or $H_2O_2$, reactions (4) and (5) can be established:

$$[Fe^{II}_4Fe^{III}_2(OH)_{12}][CO_3, 2H_2O] + O_2 \rightarrow Fe^{III}_6O_{(2+x)}(OH)_{(12-2x)} \times (H_2O)_x(CO_3) + 2H_2O \quad (4)$$

$$[Fe^{II}_4Fe^{III}_2(OH)_{12}][CO_3, 2H_2O] + 2H_2O_2 \rightarrow Fe^{III}_6O_{(2+x)} \times (OH)_{(12-2x)}(H_2O)_x(CO_3) + 4H_2O\,. \quad (5)$$

### 4.3. Stability of the Ferric Oxyhydroxycarbonate, exGr-Fe(III)

At ambient temperature and below, exGR-Fe(III) remains stable even after large periods of aging, either as a dry powder or as particles in solution. The conversion into thermodynamically stable ferric phases, goethite or hematite, occurs only in moderately heated solutions stored in glass-free containers. The formation of the latter compounds requires the occurrence of a dissolution-precipitation (D-P) mechanism (Jambor and Dutrizac, 1998). In presence of silicate or phosphate species, the dissolution step is inhibited due to the adsorption of these species onto the exGR-Fe(III) surface (Sigg and Stumm, 1981; Cornell et al., 1987), and the latter compound transformation is prevented.

### 4.4. Oxidation of GR($CO_3^{2-}$) Via Solution

At point B, the solution contains GR($CO_3^{2-}$) suspension and soluble $[(Fe^{II})_2(Fe^{III})_1]$ species (Misawa et al., 1973; Misawa et al., 1974) in equilibrium with the solid phase, as illustrated by the following schematic reaction,

$$[Fe^{II}_4Fe^{III}_2(OH)_{12}][CO_3, 2H_2O] \underset{\text{precipitation}}{\overset{\text{dissolution}}{\rightleftharpoons}} 2[(Fe^{II})_2(Fe^{III})_1]\,. \quad (6)$$

Figure 9 showed that the dissolution of GR($CO_3^{2-}$) is promoted by acid addition and that the pH range where it occurs, ~8.4, is less alkaline than the one relative to the neutralisation of $CO_3^{2-}$ species according to

$$CO_3^{2-} + H^+ \rightarrow HCO_3^-\,. \quad (7)$$

On the other hand, protons will preferentially react with $CO_3^{2-}$ (if available) rather than with GR($CO_3^{2-}$).

The introduction of oxygen into the cell at point B induces the oxidation of $[(Fe^{II})_2(Fe^{III})_1]$ species according to the schematic reaction

$$2[(Fe^{II})_2(Fe^{III})_1] + O_2 \rightarrow 6\ FeOOH + y\ H^+\,. \quad (8)$$

The production of protons associated to the oxidation of $Fe^{II}$-containing species into FeOOH is well established (Schwertmann and Cornell, 1991). In 0.04 mol/L $NaHCO_3$ solution with very slightly alkaline pH, $CO_3^{2-}$ concentration in solution is very low and reaction (7) is negligible. Then, the protons produced in Eqn. 8 can promote reaction (6) in the dissolution sense, leading to the release of fresh $[(Fe^{II})_2(Fe^{III})_1]$ species in solution. A self-sustained mechanism is observed where GR($CO_3^{2-}$) and dissolved oxygen are the reagents, FeOOH the end product, and $[(Fe^{II})_2(Fe^{III})_1]$ the intermediate species. The whole transformation is a dissolution-oxidation-precipitation (DOP) mechanism. The nature of the ferric oxihydroxide should depend on the experimental conditions; lepidocrocite predominantly formed in the present study, goethite was obtained in synthesis from Drissi et al. (1995), Schwertmann and Cornell (1991), ferrihydrite may be present along with lepidocrocite and goethite. The DOP mechanism may be extended to sulphate and chloride green rusts as the occurrence of ferrous-ferric species (green complexes) has also been reported in neutral and mildly alkaline solutions containing sulphate or chloride ions (Misawa et al., 1973; Misawa et al., 1974).

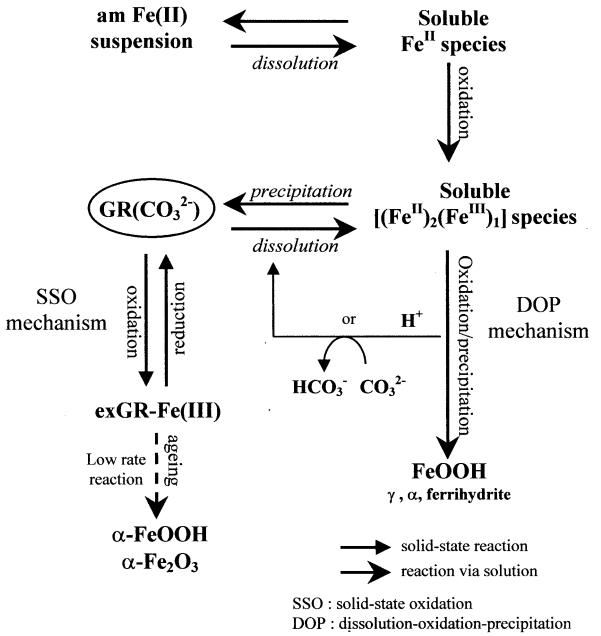


Fig. 11. Schematic representation of formation and transformation pathways of GR($CO_3^{2-}$).

### 4.5. Formation and Transformation Pathways of GR($CO_3^{2}$)

Results of the present study allow the establishment of a schematic representation for formation and transformation pathways of GR($CO_3^{2-}$) (Fig. 11). The formation of GR($CO_3^{2-}$) from amorphous Fe(II) suspension involves three steps, as proposed in section 4.1: dissolution of amorphous Fe(II) suspension, oxidation of soluble ferrous species into soluble ferrous-ferric species, and precipitation to GR($CO_3^{2-}$). The oxidation of GR($CO_3^{2-}$) can proceed by solid-state reaction (SSO) or by reaction via solution (DOP). The SSO mechanism is promoted at the expenses of the DOP mechanism (i) by increasing the $[CO_3^{2-}]/[GR(CO_3^{2-})]$ ratio, (ii) by increasing the oxidation rate, and (iii) in the presence of adsorbed blocking species such as phosphate or silicate. Condition (i) is monitored by adjusting the total concentration of carbonate species, the pH, and the concentration of iron species. Condition (ii) is related to the flow of oxygen (solution stirring) or soluble oxidising species (addition rate). Condition (iii) may be fulfilled for many soil or corrosion environments since phosphate and silicate ions are widespread species. The GR($CO_3^{2-}$) oxidation mechanism (see Introduction) proposed by Benali et al. (2001) is not consistent with the results of the present paper. In

our mind, their mechanism is quite doubtful since it is well known that the ferrihydrite-to-goethite transformation is a very slow reaction at ambient temperature (Schwertmann and Cornell, 1991; Jambor and Dutrizac, 1998). As a matter of fact, the ferric product they synthesized might be exGR-Fe(III) rather than ferrihydrite. The solid-state reduction of exGR-Fe(III) back to GR($CO_3^{2-}$) was demonstrated in our present study. This reduction process should occur with a negligible release of soluble iron species in solution, as for the oxidation process. If it occurs in natural environments, the solid-state redox cycling of GR($CO_3^{2-}$) may affect the remobilization of iron. To state, the reaction pathways described in the present study should be considered in all environments where GR($CO_3^{2-}$) occurs.

*Acknowledgments*—The authors thank the associate-editor, G. Sposito, and two of the reviewers for their helpful and valuable comments and suggestions.

*Associate editor:* G. Sposito

## REFERENCES

Abdelmoula M., Refait Ph., Drissi S. H., Mihe J. P., and Génin J. M.-R. (1996) Conversion electron Mössbauer spectroscopy and X-ray diffraction studies of the formation of carbonate-containing green rust one by corrosion of metallic iron in $NaHCO_3$ and ($NaHCO_3$ + NaCl) solutions. *Corros. Sci.* **38,** 623–633.

Allmann R. (1968) The crystal structure of pyroaurite. *Acta Cryst.* **B24,** 972–977.

Benali O., Abdelmoula M., Refait Ph., and Génin J. M.-R. (2001) Effect of orthophosphate on the oxidation product of Fe(II)-Fe(III) hydroxycarbonate. The transformation of green rust to ferrihydrite. *Geochim. Cosmochim. Acta* **65,** 1715–1726.

Bernal J. D., Dasgupta D. R., and Mackay A. L. (1959) The oxides and hydroxides of iron and their structural inter-relationships. *Clay Miner. Bull.* **4,** 15–30.

Bonin P. M., Jedral W., Odziemkowski M. S., and Gillham R. W. (2000) Electrochemical and Raman spectroscopic studies of the influence of chlorinated solvents on the corrosion behaviour of iron in borate buffer and in simulated groundwater. *Corros. Sci.* **42,** 1921–1939.

Butler G. and Beynon J. G. (1967) The corrosion of mild steel in boiling salt solutions. *Corros. Sci.* **7,** 385–404.

Cornell R. M., Giovanoli R., and Schindler P. W. (1987) Effect of silicate species on the transformation of ferrihydrite into goethite and hematite in alkaline media. *Clays Clay Miner.* **35,** 21–28.

Chukhrov F. V., Zvyagin B. B., Gorshkov A. I., Ermilova L. P., Korovushkin V. V., Rudnitskaya Y. E., and Yakubovskaya N. Y. (1977) Feroxyhyte, a new modification of FeOOH. *Int. Geol. Rev.* **19,** 873–890.

Detournay J., Derié R., and Ghodsie M. (1975) The region of stability of GR II in the electrochemical potential-pH diagram in sulphate medium. *Corros. Sci.* **15,** 295–306.

Detournay J., Dérié R., and Ghodsie M. (1976) Etude de l'oxydation par aération de $Fe(OH)_2$. *Z. Anorg. Allg. Chem.* **427,** 265–273.

Drissi S. H., Refait Ph., Abdelmoula M., and Génin J. M. R. (1995) The preparation and thermodynamic properties of Fe(II)-Fe(III) hydroxide-carbonate (green rust 1); Pourbaix diagram of iron in carbonate-containing aqueous media. *Corros. Sci.* **37,** 2025–2041.

Erbs M., Hansen H. C. B., and Olsen C. E. (1999) Reductive dechlorination of carbon tetrachloride using iron(II) iron(III) hydroxide sulfate (green rust). *Environ. Sci. Technol.* **33,** 307–311.

Erdös V. E. and Altorfer H. (1976) Ein dem Malachit ähnliches basisches Eisenkarbonat als Korrosiosprodukt von Stahl. *Werkstoffe und Korrosion* **27,** 304–312.

Feitknecht W. and Keller G. (1950) Über die Dunkelgrünen Hydroxyverbindungen des eisens. *Z. Anorg. Allg. Chem.* **262,** 61–68.

Fredrickson J. K., Zachara J. M., Kennedy D. W., Dong H., Onstott T. C., Hinman N., and Li S. M. (1998) Biogenic iron mineralization accompanying the dissimilatory reduction of hydrous ferric oxide by a groundwater bacterium. *Geochim. Cosmochim. Acta* **62,** 3239–3257.

Géhin A., Ruby C., Abdelmoula M., Benali O., Ghanbaja J., Refait Ph., and Génin J. M.-R. (2002) Synthesis of Fe(II-III) hydroxysulphate green rust by coprecipitation. *Solid State Sci.* **4,** 61–66.

Génin J. M. R., Olowe A. A., Résiak B., Benbouzid-Rollet N. D., Confente M. and Prieur D. (1993) Identification of sulphated green rust 2 compound produced as a result of microbially induced corrosion of steel sheet piles in harbour. In *Marine Corrosion of Stainless Steels: Chlorination and Microbial Effects, European Federation Corrosion Series n°10, The Institute of Materials, London,* **10,** 162–166.

Génin J. M. R., Olowe A. A., Refait Ph., and Simon L. (1996) On the stoichiometry and Pourbaix diagram of Fe(II)-Fe(III) hydroxy-sulphate or sulphate-containing green rust 2: an electrochemical and Mössbauer spectroscopy study. *Corros. Sci.* **38,** 1751–1762.

Génin J. M. R., Refait Ph., Simon L., and Drissi S. H. (1998) Preparation and Eh-pH diagrams of Fe(II)-Fe(III) green rust compounds; hyperfine interaction characteristics and stoichiometry of hydroxychloride, -sulphate and –carbonate. *Hyp. Interact.* **111,** 313–318.

Hansen H. C. B. (1989) Composition, stabilization, and light absorption of Fe(II)Fe(III) hydroxy-carbonate ("green rust"). *Clay Miner.* **24,** 663–669.

Hansen H. C. B. and Bender Koch C. (1998) Reduction of nitrate to ammonium by sulphate green rust: activation energy and reaction mechanism. *Clay Minerals* **33,** 87–101.

Jambor J. L. and Dutrizac J. E. (1998) Occurrence and constitution of natural and synthetic ferrihydrite, a widespread iron oxyhydroxide. *Chem. Rev.* **98,** 2549–2585.

Legrand L., Savoye S., Chaussé A., and Messina R. (2000) Study of oxidation products formed on iron in solutions containing bicarbonate/carbonate. *Electrochim. Acta* **46,** 111–117.

Legrand L., Abdelmoula M., Géhin A., Chaussé A., and Génin J. -M. R. (2001a) Electrochemical formation of a new Fe(II)-Fe(III) hydroxy-carbonate green rust: characterisation and morphology. *Electrochim. Acta* **46,** 1815–1822.

Legrand L., Sagon G., Lecomte S., Chaussé A., and Messina R. (2001b) A. Raman and infrared study of a new carbonate green rust obtained by electrochemical way. *Corros. Sci.* **43,** 1739–1749.

Legrand L., Maksoub R., Sagon G., Lecomte S., Dallas J. P., and Chaussé A. (2003) Electroanalytical and kinetic investigations on the carbonate green rust –Fe(III) redox system. *J. Electrochem. Soc.* **150,** B45–B51.

Lindsay W. L. (1979) *Chemical Equilibria In Soils*. Wiley Interscience.

Loyaux-Lawniczak S., Refait Ph., Ehrhardt J. J., Lecomte P., and Génin J. M. R. (2000) Trapping of Cr by formation of ferrihydrite during the reduction of chromate ions by Fe(II)-Fe(III) hydroxysalt green rusts. *Environ. Sci. Technol.* **34,** 438–443.

McGill I. R., McEnaney B., and Smith D. C. (1976) Crystal structure of green rust formed by corrosion of cast iron. *Nature* **259,** 1521–1529.

Markov L., Blaskov V., Klissurski D., and Nikolov S. (1990) The thermal decomposition mechanism of Iron(III) hydroxide carbonate to $\alpha$-$Fe_2O_3$. *J. Mater. Sci.* **25,** 3096–3100.

Misawa T., Hashimoto K., and Shimodaira S. (1973) Formation of $Fe(II)_1$-$Fe(III)_1$ intermediate green complex on oxidation of ferrous ion in neutral and slightly alkaline sulphate solutions. *J. Inorg. Nucl. Chem.* **35,** 4167–4174.

Misawa T., Hashimoto K., and Shimodaira S. (1974) The mechanism of formation of iron oxide and oxyhydroxides in aqueous solutions at room temperature. *Corros. Sci.* **14,** 131–149.

Olowe A. A. and Génin J. M. R. (1991) The mechanism of oxidation of Fe(II) hydroxide in sulphated aqueous media: importance of the initial ratio of the reactants. *Corros. Sci.* **32,** 965–984.

Ona-Nguema G., Abdelmoula M., Jorand F., Benali O., Géhin A., Block J. C., and Génin J. M. R. (2002) Iron (II, III) hydroxycarbonate green rust formation and stabilization from lepidocrocite bioreduction. *Environ. Sci. Technol.* **36,** 16–20.

Peulon S., Legrand L., Antony H. and Chaussé A. (2003) Electrochemical deposition of thin films of green rusts 1 and 2 on inert gold substrate. *Electrochem. Comm.* **5,** 208–213.

Ponnamperuma F. N. (1972) The chemistry of submerged soils. *Adv. In Agronomy* **24,** 173–189.
Refait Ph. and Génin J. M. R. (1993) The oxidation of Fe(II) hydroxide in chloride-containing aqueous media and Pourbaix diagrams of green rust I. *Corros. Sci.* **34,** 797–819.
Refait Ph., Simon L., and Génin J. M. R. (2000) Reduction of $SeO_4^{2-}$ anions and anoxic formation of iron(II)-iron(III) hydroxy-selenate green rust. *Environ. Sci. Technol.* **34,** 819–825.
Savoye S., Legrand L., Sagon G., Lecomte S., Chaussé A., Messina R., and Toulhoat P. (2001) Experimental investigations on iron corrosion products formed in bicarbonate/carbonate-containing solutions at 90°C. *Corros. Sci.* **43,** 2049–2064.
Schwertmann U. and Cornell R. M. (1991) *Iron Oxides In the Laboratory: Preparation and Characterization*. VCH Publishers, Inc..
Schwertmann U. and Fechter H. (1994) The formation of green rust and its transformation to lepidocrocite. *Clay Miner.* **29,** 87–92.
Sigg L. and Stumm W. (1981) The interactions of anions and weak acids with the hydrous goethite ($\alpha$-FeOOH) surface. *Colloïd. Surfaces* **2,** 101–117.
Stampfl P. P. (1969) Ein basisches Eisen II-III Karbonat in Rost. *Corros. Sci.* **9,** 185–187.
Taylor R. M. (1980) Formation and properties of Fe(II)-Fe(III) hydroxycarbonate and its possible significance in soil formation. *Clay Miner.* **15,** 369–382.
Towe K. M. and Bradley W. F. (1967) Mineralogical constitution of colloïdal "hydrous ferric oxide." *J. Colloïd. Interface Sci.* **24,** 384–392.
Trolard F., Génin J. -M. R., Abdelmoula M., Bourrié G., Humbert B., and Herbillon A. (1997) Identification of a green rust mineral in a reductomorphic soil by Mössbauer and Raman spectroscopies. *Geochim. Cosmochim. Acta* **61,** 1107–1111.
Weckler B. and Lütz H. D. (1998) Lattice vibration spectra. Part XCV. Infrared spectroscopic studies on the iron oxide hydroxides goethite ($\alpha$), akaganéite ($\beta$), lepidocrocite ($\gamma$), and feroxyhite ($\delta$). *Eur. J. Solid State Inorg. Chem.* **35,** 531–544.
Williams A. G. B. and Scherer M. M. (2001) Kinetics of Cr(VI) reduction by carbonate green rust. *Environ. Sci. Technol.* **35,** 3488–3494.

## APPENDIX

### Chemical Composition of Carbonate Green Rust GR($CO_3^{2-}$)

$Fe^{II}$ content 66%; average total iron content ($Fe^{II}$ + $Fe^{III}$) 52.1% wt; $CO_3$ content 7.91% wt.

Calculations for 100 g:

$$n(Fe^{II})=0.616 \text{ mole}; \; n(Fe^{III})=0.317 \text{ mole}; \; n(CO_3)=0.132 \text{ mole}$$

Charge balance and mass balance

$$n(OH)=2\,n(Fe^{II}) + 3\,n(Fe^{III}) - 2\,n(CO_3) = 1.919 \text{ moles}$$

$$n(H_2O) = [100 - 55.85\,n(Fe^{II}) - 55.85\,n(Fe^{III}) - 60\,n(CO_3) - 17\,n(OH)]/18 = 0.408 \text{ mole}$$

The chemical composition is then determined for 6 Fe atoms

### Chemical Composition of Ferric Oxyhydroxycarbonate ExGR-Fe(III)

$Fe^{II}$ content 0%; average total iron content ($Fe^{III}$) 51.8% wt; $CO_3$ content 6.82% wt.

Calculations for 100 g:

$$n(Fe^{III}) = 0.927 \text{ mole} \; ; \; n(CO_3) = 0.114 \text{ mole}$$

Charge balance and mass balance

$$3\,n(Fe^{III}) - 2\,n(CO_3) - 2\,n(O) + n(H) = 0$$

$$55.85\,n\,(Fe^{III}) + 60\,n(CO_3) + 16\,n(O) + 1\,n(H) = 100$$

$$n(O) = 2.227 \text{ mole}; \; n(H) = 1.900$$

The chemical composition is then determined for 6 Fe atoms.